




# CT and clinical features for distinguishing endophytic clear cell renal cell carcinoma from urothelial carcinoma

Xin Chen   
Yidi Chen   
Yiwu Leia   
Fuling Huang   
Cheng Tanga   
Liling Longa 

## PURPOSE

We aimed to characterize the clinical and multiphase computed tomography (CT) features of the distinguishing endophytic clear cell renal cell carcinoma (ECCRCC) from endophytic renal urothelial carcinoma (ERUC).

## METHODS

Data from 44 patients (35 men and 9 women) with ECCRCC and 21 patients (17 men and 4 women) with ERUC were retrospectively assessed. The mean patient age was 55 years (48.25-59.50 years) and 68 years (63.00-73.00 years), respectively. Univariate and multivariate logistic regression analyses were performed to determine independent predictors for ECCRCC and to construct a predictive model that comprised clinical and CT characteristics for the differential diagnosis of ECCRCC and ERUC. Differential diagnostic performance was assessed using the area under the receiver operating characteristic curve (AUC).

## RESULTS

The independent predictors of ECCRCC were heterogeneous enhancement (odds ratio [OR]=0.027,  $P=.005$ ), hematuria (OR for gross hematuria=53.995,  $P=.003$ ; OR for microscopic hematuria=31.126,  $P=.027$ ), and an infiltrative growth pattern (OR=24.301,  $P=.022$ ). The AUC of the predictive model was 0.938 ( $P<.001$ , sensitivity=84.10%, specificity=95.20%), which had a better diagnostic performance than heterogeneous enhancement (AUC=0.766,  $P=.001$ , sensitivity=81.82%, specificity=71.43%), hematuria (AUC=0.786,  $P<.001$ , sensitivity=81.82%, specificity=66.67%), and infiltrative growth pattern (AUC=0.748,  $P=.001$ , sensitivity=90.48%, specificity=59.09%).

## CONCLUSION

The independent predictors, as well as the predictive model of CT and clinical characteristics, may assist in the differential diagnosis of ECCRCC and ERUC and provide useful information for clinical decision-making.

Renal cell carcinoma (RCC) is the most common malignant renal tumor,<sup>1</sup> and 70%-80% of RCC cases are clear cell renal cell carcinoma (ccRCC).<sup>2-5</sup> ccRCCs are usually exophytic renal masses, wherein the tumor center is located in the renal parenchyma or extrarenal fat. However, ccRCCs may also be endophytic masses and may mimic endophytic renal urothelial carcinoma (ERUC).<sup>6,7</sup> Because of their different treatments<sup>8</sup> and prognoses, the preoperative differentiation of endophytic clear cell renal cell carcinoma (ECCRCC) and ERUC via computed tomography (CT) is challenging for urologists. Similarly, the same location of tumors makes it difficult to distinguish ECCRCC from ERUC before surgery using CT.<sup>9,10</sup> Raza et al.<sup>9</sup> expanded the definition of central RCC. Their study included some exophytic RCCs and RCCs in the renal pelvis. Moreover, their study included RCC subtypes other than ccRCC. Bata et al.<sup>10</sup> compared the CT values of dynamic enhancement between urothelial carcinoma (UC) and ccRCC, without considering the morphological characteristics of CT imaging.

Moreover, endophytic RCCs represent collecting system invasion (CSI), which reportedly results in a poor prognosis.<sup>11-14</sup> A few radiologists have begun to study the CT features of CSI. Karlo et al.<sup>11</sup> compared the results of CT-based diagnosis and pathological diagnosis

From the Department of Radiology (X.C. ✉ 23825633@qq.com, Y.L., F.H., C.T., L.L. ✉ cjr.longliling@vip.163.com), The First Affiliated Hospital of Guangxi Medical University, Nanning, China; Department of Radiology (Y.C.), West China Hospital, Sichuan University, Sichuan, China.

Received 25, December 2022 revision requested 28, January 2022 last revision received 11, May 2022 accepted 20, June 2022.

Publication date: 5 October 2022.

DOI: 10.5152/dir.2022.211248

You may cite this article as: Chen X, Chen Y, Leia Y, Huang F, Tanga C, Longa L. CT and clinical features for distinguishing endophytic clear cell renal cell carcinoma from urothelial carcinoma. *Diagn Interv Radiol.* 2022;28(5):410-417.

of CSI. Takamatsu et al.<sup>15</sup> explored the correlation between the CT signs of CSI and the survival rate. However, to the best of our knowledge, there are no published studies specifically on CT-based diagnosis to differentiate between ECCRCC and ERUC.

The clinical history and the patient's symptoms are important in the diagnosis of RCC and upper urinary tract UC. Smoking is a risk factor for both RCC and upper urinary tract UC.<sup>16,17</sup> Further, kidney stones may be associated with upper urinary tract UC.<sup>18,19</sup> Flank pain and hematuria are considered typical symptoms of both ccRCC<sup>20</sup> and upper urinary tract UC.<sup>21,22</sup> Neither Raza et al.<sup>9</sup> nor Bata et al.<sup>10</sup> determined the correlation between clinical data and CT for the differential diagnosis of ECCRCC and ERUC.

Therefore, we aimed to retrospectively assess and adequately describe the CT characteristics of ECCRCC and ERUC and to determine their correlations with clinical data.

## Methods

This study was approved by our institutional research ethics committee (protocol number: 2021 [KY-E-214]), who waived the need for informed patient consent.

### Patients

Patients with UC or ccRCC, who had undergone surgery or biopsy in our hospital from August 2008 to December 2020, were involved, and their data were retrospectively analyzed. All the patients underwent a multiphase CT scan within 1 week before surgery or biopsy. Patients with ERUC or ECCRCC who also had other tumor components and patients with tuberculous or a purulent infection were excluded. Patients with exophytic solid ccRCCs and cystic-dominant ccRCCs were also excluded.<sup>23</sup> Patients with combined masses of the ureter or bladder were

excluded. Finally, patients with diffuse UCs with hydronephrosis and exophytic renal UC were excluded (Figure 1).

### Clinical and pathological data

Clinical data of included patients were collected using the hospital information system (DHC Software Co), which included age, sex, smoking history, flank pain, kidney stone history, and hematuria. Patients with a smoking history of more than 20 years and no less than a pack of cigarettes per day were considered as having a positive smoking history.<sup>16,17</sup> Patients who had had kidney stones for more than 5 years were considered to have a positive history of kidney stones. Cases with asymptomatic small calculi or microcalculi were not considered positive.<sup>18,19</sup> A patient was considered positive for microscopic hematuria if the result for occult blood in routine urine tests was positive, without visible blood. Pathology reports were obtained from the picture archiving and communication system (PACS) (Shenzhen Annet Information System Co. Ltd). Histological slides from all included patients were reviewed for

this study. The final pathological diagnosis was established by 2 pathologists (each with 10 years of experience in diagnosing renal diseases) via combined microscopic and immunohistochemical examination (ccRCC: vimentin [+], CD10 [+], RCC Ma [+], PAX-8 [+]; UC: CK7 [+], P63 [+], CK20 [+/-]), and any differences were arbitrated by another senior pathologist who was blinded to the study information.

### Computed tomography scanning

Patients underwent multiphase CT scanning, including an unenhanced phase (UP) scan, and contrast enhancement scanning of the corticomedullary phase (CP), nephrographic phase (NP), and excretory phase (EP). Patients were scanned using 16-slice, 64-slice, 128-slice, and 256-slice spiral CT (Light Speed VCT and Revolution, GE Healthcare; SOMATOM sensation 16, SOMATOM Definition Flash, and SOMATOM Force, Siemens Healthcare). The scanning area was from the top of the diaphragm to the level of the iliac wing. The scanning parameters were as follows: tube voltage, 120 kV; tube current, 250-300 mA; and

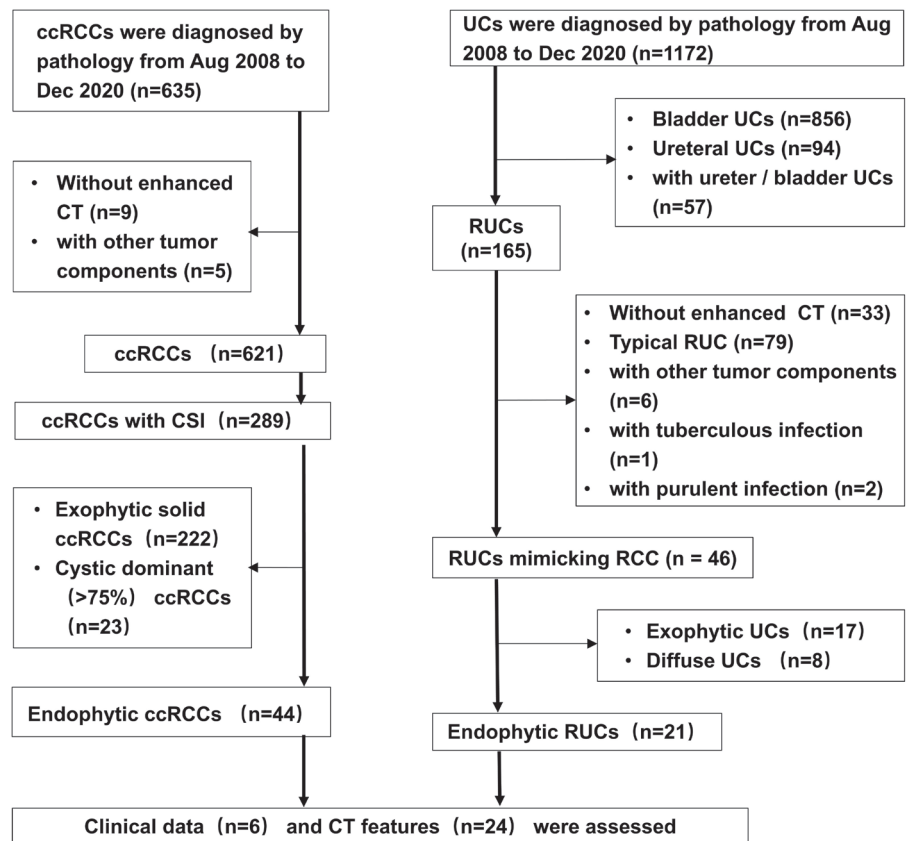


**Figure 1.** Flowchart for inclusion and exclusion of patients. ccRCC, clear cell renal cell carcinoma; CT, computed tomography; RCC, renal cell carcinoma; RUC, renal urothelial carcinoma; UC, urothelial carcinoma.

### Main points

- Endophytic clear cell renal cell carcinoma (ECCRCC) and endophytic renal urothelial carcinoma (ERUC) have different computed tomographic (CT) characteristics and clinical features.
- ECCRCC can be distinguished from ERUC by using CT characteristics and clinical data.
- A predictive model may improve the differential diagnosis of ECCRCC and ERUC.

slice thickness, 5 mm. After the abdominal plain scan, a contrast agent (Iopamiro, 300 mgI/mL; Shanghai Bracco Sine Pharmaceutical Corp. Ltd.) was injected using a high-pressure syringe around the median cubital vein, with an injection flow rate of 3 mL/s. Contrast-enhanced CT scans were performed at 25-30 seconds (renal cortex phase), 75-85 seconds (NP), and 210-280 seconds (EP).

### Imaging analysis

All CT images were obtained from the PACS of our hospital (Shenzhen Annet Information System Co. Ltd). The maximum tumor diameter was measured only in the axial direction. The CT features analyzed included the location, size, infiltrative growth pattern, renal calculi, hydronephrosis, necrosis, and enhancement pattern. ccRCC with CSI was defined as follows according to Karlo et al.<sup>11</sup>: a tumor causing a filling defect in the EP, a tumor in contact with the collecting system on the CT image, and/or a tumor separated from the collecting system. Renal urothelial carcinoma (RUC) mimicking RCC was defined as a UC that was difficult to diagnose as a renal pelvic carcinoma via CT urography, which is the method of choice for imaging-based diagnosis of upper urinary tract UC according to the European Association of Urology Guidelines.<sup>8</sup> As described by Gervais et al.,<sup>2</sup> we defined endophytic renal tumors as the tumors centrally located in the renal pelvis. Necrosis was defined as areas of low attenuation or non-enhancement in the tumor that were not sharply demarcated and lacked apparent walls, according to Shinagare et al.<sup>24</sup> As described by Dyer et al.,<sup>25</sup> we defined solid renal mass infiltrative growth patterns as bean-shaped (tumor infiltrative growth using renal parenchyma as scaffold) and ball-shaped (dominant tumor expansion growth). Hyperenhancement and hypoenhancement were defined as  $\geq 70$  Hounsfield units (HU) or 20-40 HU of absolute enhancement, respectively, in the CP.<sup>23</sup> We used the definition of Pano et al.<sup>26</sup> for heterogeneous/homogeneous enhancement, that is, tumors with non-enhancing or low-attenuation areas were described as heterogeneous, and tumors that enhanced uniformly were described as homogeneous, throughout the visual assessment in the soft-tissue window. Referring to the report by Jung et al.,<sup>27</sup> we set the window width to 300 and the window level to 40. Heterogeneous/homogeneous

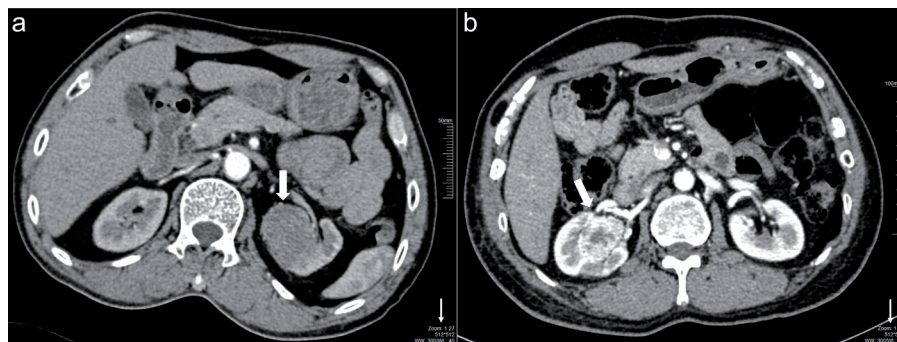


**Figure 2.** Definition of heterogeneous enhancement. Axial image in the corticomedullary phase showing a homogeneously enhanced tumor (ERUC) in the left kidney (*white arrow*). The attenuation of ERUC is uniform throughout the visual assessment (a). Axial image in the corticomedullary phase showing a heterogeneously enhanced tumor (ECCRCC) in the right kidney (*white arrow*). The attenuation of the ECCRCC is non-uniform throughout the visual assessment. Low attenuation is evident in the ECCRCC center. Low attenuation contrasts sharply with the high attenuation around it (b). Both panels have the same window width and window level (*thin white arrow*). ECCRCC, endophytic clear cell renal cell carcinoma; ERUC, endophytic renal urothelial carcinoma.

enhancement was visually assessed with the same window settings (Figure 2). In every patient, as per Bata et al.,<sup>10</sup> 3 circular regions of interest (ROIs) of the same size (10 mm<sup>2</sup>) were drawn in the most homogeneous solid area of every tumor, and the average of the triplicate values was used as the average CT value of the tumor in each phase (Figure 3). We avoided not only areas with cystic necrosis, blood vessels, calcification, and stones but also the adjacent renal parenchyma. Attenuation values in each phase were described in HU. The images were assessed by 2 radiologists (each with more than 10 years of experience in abdominal CT diagnosis) who were blinded to the study information, and differences between them were arbitrated by another senior radiologist who was similarly blinded.

### Statistical analyses

Statistical analyses were performed using International Business Machines Statistical Package for the Social Sciences program for Windows version 22.0 (IBM Corp.). The kappa coefficient and intraclass correlation coefficient were used to calculate the inter-rater agreement of the two readers (Supplementary Tables 1 and 2). Descriptive statistics of categorical data are presented as n (%). Non-normalized variables were presented as median (range), and normally distributed variables were represented as the mean  $\pm$  standard deviation. We evaluated the data distribution for normality with the Kolmogorov-Smirnov and Shapiro-Wilk tests. Student t test/Mann-Whitney U test was used to compare continuous variables, and the chi-square test/Fischer exact test was used to compare categorical variables.

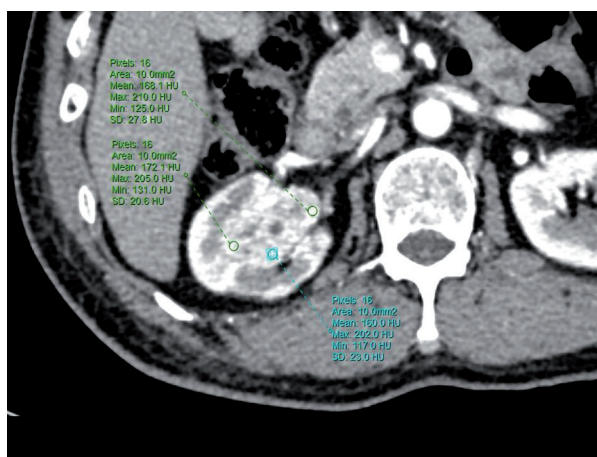


**Figure 3.** Schematic figure of drawing ROIs. Axial image in the corticomedullary phase showing a heterogeneously enhanced ECCRCC in the right kidney. Three ROIs of the same size (10 mm<sup>2</sup>) were drawn in the most homogeneous solid areas of the tumor. Areas with cystic necrosis, blood vessels, calcification, and stones were avoided, as well as the adjacent renal parenchyma. ROI, region of interest.

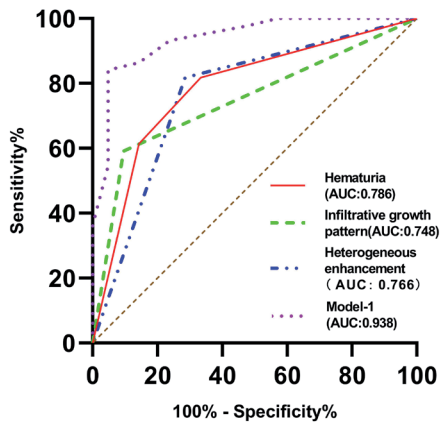


**Figure 4.** ROC curves of the CT and clinical characteristics to distinguish ECCRCC from ERUC. AUC, area under the curve; model-1 =  $1/[1 + e^{-(-3.831 \text{ gross hematuria} + 3.206 \text{ microscopic hematuria} + 2.783 \text{ infiltrative growth pattern} - 3.416 \text{ heterogeneous enhancement} - 0.698)}]$ ; ROC, receiver operating characteristic.

Clinical data and CT features of ECCRCC and ERUC are summarized in Supplementary Tables 3 and 4, respectively.

Subsequently, variables with statistically significant differences were evaluated using the receiver operating characteristic (ROC) curve analysis. The cutoff value was determined by calculating the maximum Youden index. Variables in the ROC curve analysis with an area under the curve (AUC) < 0.7 (low accuracy) were excluded, according to Swets.<sup>28</sup> Next, the variables with statistically significant differences were analyzed using univariate logistic regression for associations with ERUC or ECCRCC. We assigned values for variables before we commenced logistic regression analysis (Supplementary Table 5). Then, we attempted to avoid over-fitting the ROC curve of the predictive model by excluding variables with odds ratios close to 1 (reflecting a weak association) from the multivariate logistic regression analysis.<sup>29-31</sup> The rest of the

variables were analyzed using multivariate logistic regression. Statistically significant variables (independent predictors) were used in the multivariate logistic regression analysis to construct the predictive model (Supplementary Equation 1).<sup>32</sup> A Hosmer–Lemeshow test was used to assess the statistical significance of the model. Ultimately, ROC curves were drawn based on the independent predictors and the predictive model to evaluate and compare the diagnostic performance of CT characteristics and clinical features for ERUC and ECCRCC. Statistical significance was set at  $P < .05$ .

## Results

All kappa and intraclass correlation coefficient values were >0.8 (Supplementary Tables 1 and 2; hence, there was excellent agreement between the 2 readers. All continuous variables were non-normally distributed, except for the UP.

Results of the clinical characteristics are summarized in Supplementary Table 3. This study included 44 patients with ECCRCC (with CSI) (35 men and 9 women) and 21 patients with ERUC (mimicking RCC) (17 men and 4 women). No significant difference was found between sex, smoking history, and history of kidney stones among the groups ( $P = 1.000$ ,  $P = .913$ , and  $P = .214$ , respectively). The median patient age was 55 years (48.25–59.50 years) and 68 years (63.00–73.00 years) in the ECCRCC and ERUC groups, respectively ( $P < .001$ ). The frequency of flank pain differed ( $P = .034$ ) between the ECCRCC (17 patients, 38.64%) and ERUC (14 patients, 66.67%) groups. The distribution of hematuria classification also differed ( $P < .001$ ) between ECCRCC (8 [18.18%] with gross hematuria and 9 [20.45%] with microscopic hematuria) and

ERUC (14 [66.67%] with gross hematuria and 4 [19.05%] with microscopic hematuria) groups.

Results of CT features are summarized in Supplementary Table 4. No differences were observed among the side, preserving reniform contour, perinephric stranding, calcification, renal vein invasion, lymphatic node metastasis, and distant metastasis between the groups ( $P = .386$ ,  $P = .993$ ,  $P = .095$ ,  $P = .133$ ,  $P = .180$ ,  $P = .200$ , and  $P = .200$ , respectively). The median tumor size was 43.20 cm (32.70–68.70 cm) and 44.37 cm (33.32–59.20 cm) between the groups, respectively ( $P = .768$ ). The mean UP CT values were  $36.67 \pm 6.02$  HU and  $36.25 \pm 3.68$  HU in ERCCCs and ERUCs, respectively ( $P = .063$ ). The infiltrative growth pattern differed ( $P < .001$ ) between the ECCRCC (18 tumors [40.91%] with a bean shape and 26 [59.09%] with a ball shape) and ERUC (19 tumors [90.48%] with a bean shape and 2 [9.52%] with a ball shape) groups. The pseudo-capsule sign was more common ( $P = .002$ ) in the ECCRCC group (22 patients, 50.00%) than in the ERUC group (2 patients, 9.52%). Hydronephrosis was less common ( $P = .003$ ) in the ECCRCC group (9 patients, 20.45%) than in the ERUC group (12, 57.14%). The extent of necrosis differed ( $P = .015$ ) between ECCRCC (17 patients [38.64%] with extensive necrosis and 17 [38.64%] with local necrosis) and ERUC (1 patient [4.76%] with extensive necrosis and 14 [66.67%] with local necrosis) groups. Renal calculi ( $P = .019$ ) were less common in the ECCRCC group ( $n = 5$ , 11.36%) than in the ERUC group ( $n = 8$ , 38.10%). Heterogeneous enhancement ( $P < .001$ ) was more common in the ECCRCC group ( $n = 36$ , 81.82%) than in the ERUC group ( $n = 6$ , 28.57%; CP [ $P < .001$ ], NP [ $P < .001$ ], and EP [ $P = .002$ ]). The median CT value of ECCRCC in each phase of enhancement

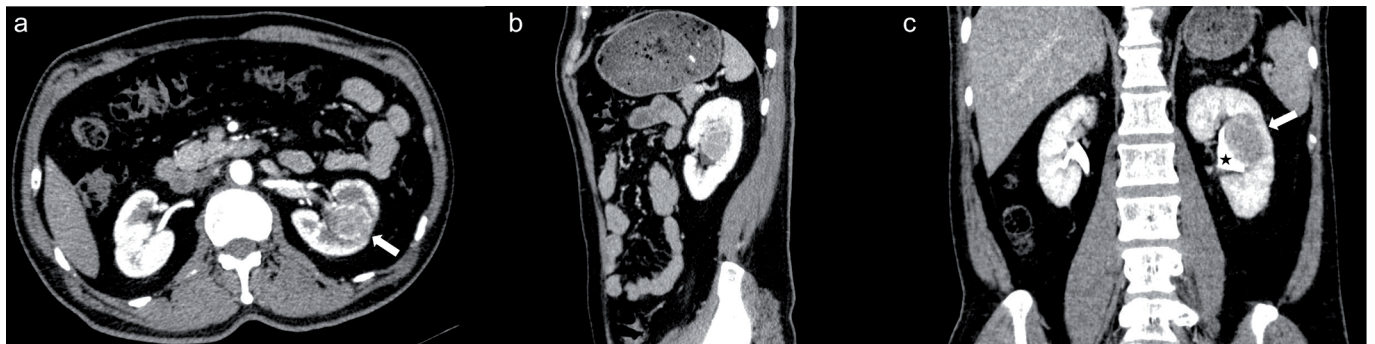


**Figure 5.** A 62-year-old man with ECCRCC. Contrast-enhanced CT. Axial image in the corticomedullary phase (a), the sagittal image in the nephrogenic phase (b), and the coronal image in the excretory phase (c) showing an endophytic, distinct, heterogeneously enhanced, ball-shaped mass in the left kidney, with a clear boundary, a pseudo-capsule sign around the tumor (white arrow), and with the renal pelvis deformed by compression (black star).

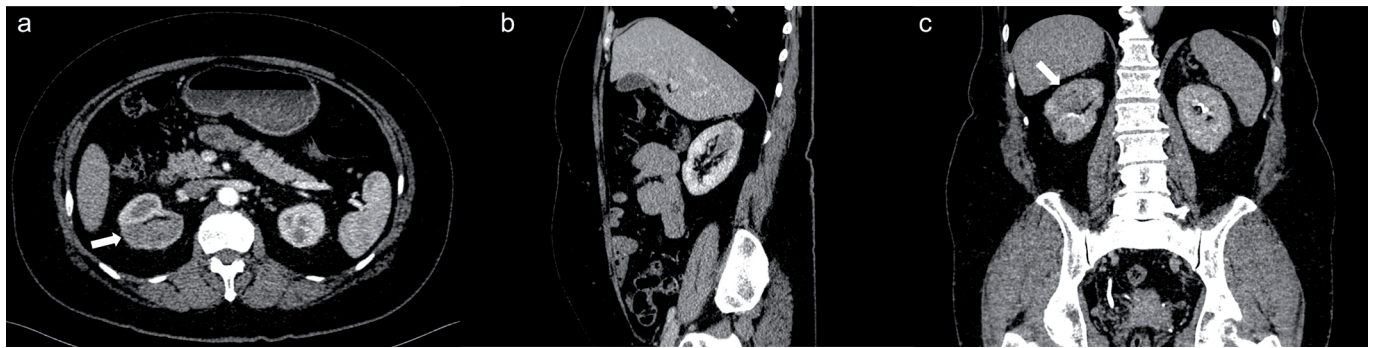


**Figure 6.** A 69-year-old woman with ERUC. Contrast-enhanced CT. Axial image in the corticomedullary phase (a), the sagittal image in the nephrogenic phase (b), and coronal image in the excretory phase (c) showing an endophytic, homogeneously enhanced mass in the right kidney (white arrow), with infiltrative growth in the renal parenchyma. The interface between the tumor and the adjacent renal parenchyma was poorly defined.

(103.07 HU [82.6-126.08 HU], 94.76 HU [79-110.76 HU], and 73.70 HU [66.74-87.54 HU]) was significantly higher ( $P < .001$ ,  $P < .001$ , and  $P = .002$ ) than that of ERUC group (62.59 [54.64-66.7], 77.94 [65.76-79.68], and 64.75 [58.43-73.49]). The ECCRCC group was prone to exhibit hyperenhancement in the CP (Figures 2b, 3, and 5), while the ERUC group was prone to hypoenhancement in the CP (Figures 2a and 6). The ERUC group was more prone to infiltrative growth in the renal parenchyma as well as hydronephrosis and renal calculus. On the other hand, the ECCRCC group more commonly exhibited heterogeneous enhancement, the pseudo-capsule sign, and necrosis (Figures 2b, 3, and 5).

In the multivariate logistic regression analysis, we did not include necrosis ( $P = .054$ ), flank pain ( $P = .069$ ), or renal calculi ( $P = .083$ ) as they did not

exhibit statistically significant differences upon ROC curve analysis. Next, hydronephrosis (AUC=0.683,  $P = .017$ ) was also excluded because its AUC < 0.7 (Table 1). Then, age (OR=0.894, 95% CI: 0.839-0.953,  $P = .001$ ), CP (OR=1.142, 95% CI: 1.062-1.229,  $P < .001$ ), NP (OR=1.095, 95% CI: 1.039-1.155,  $P = 0.001$ ), and EP (OR=1.098, 95% CI: 1.028-1.173,  $P = .005$ ) were excluded since their OR values being close to 1. The logistic regression results are presented in Table 2. Ultimately, heterogeneous enhancement, hematuria, infiltrative growth pattern, and the pseudo-capsule sign were included in the multivariate logistic regression analysis (Table 2). The independent predictors of ECCRCC including heterogeneous enhancement (OR=0.027, 95% CI: 0.002-0.342,  $P = .005$ ), hematuria (for gross hematuria, OR=53.995, 95% CI:

3.987-731.168,  $P = .003$ ; for microscopic hematuria, OR=31.126, 95% CI: 1.490-650.085,  $P = .027$ ), and infiltrative growth pattern (OR=24.301, 95% CI: 1.586-372.402,  $P = .022$ ) (Table 2) were used to construct the predictive model (model-1). According to Supplementary Table 6, the probabilistic predictive value is  $P = 1 / [1 + e^{-(-3.831 \text{ gross hematuria} + 3.206 \text{ microscopic hematuria} + 2.783 \text{ infiltrative growth pattern} - 3.416 \text{ heterogeneous enhancement} - 0.698)}]$ . The Hosmer–Lemeshow test revealed that the fitting equation of the model did not differ ( $P = .940$ ) from the real equation. The ROC curves of heterogeneous enhancement (AUC=0.766, sensitivity=81.82%, specificity=71.43%,  $P = .001$ ), hematuria (AUC=0.786, sensitivity=81.82%, specificity=66.67%,  $P < .001$ ), the infiltrative growth pattern (AUC=0.748, sensitivity=90.48%, specificity=59.09%,  $P = .001$ ), and model-1

**Table 1.** ROC analysis results of clinical and CT features for diagnosis of ECCRCC

Variables	Cutoff	AUC	SE	P	Sensitivity	Specificity	95% CI
Hematuria	1.500	0.786	0.062	<.001	66.67	81.82	0.665-0.907
Heterogeneous enhancement	0.500	0.766	0.069	.001	81.82	71.43	0.635-0.898
Infiltrative growth pattern	0.500	0.748	0.063	.001	90.48	59.09	0.626-0.869
Pseudo-capsule	0.500	0.702	0.067	.009	50.00	90.48	0.574-0.831
Hydronephrosis	0.500	0.683	0.076	.017	57.14	79.55	0.538-0.829
Necrosis	1.500	0.649	0.068	.054	38.64	95.24	0.516-0.782
Flank pain	0.500	0.640	0.080	.069	66.67	61.36	0.496-0.785
Calculus	0.500	0.634	0.075	.083	38.10	88.64	0.481-0.787
CP	74.950	0.936	0.030	<.001	86.36	95.24	0.876-0.995
NP	80.150	0.813	0.053	<.001	72.73	80.95	0.711-0.915
EP	66.350	0.742	0.064	.002	79.55	60.00	0.617-0.867
Age	62.500	0.793	0.067	<.001	81.00	84.10	0.666-0.922
Model-1	0.878	0.938	0.031	<.001	84.10	95.20	0.877-0.999

ROC, receiver operating characteristic; CT, computed tomography; ECCRCC, endophytic clear cell renal cell carcinoma; AUC, area under the receiver operating characteristic curve; SE, standard error; CI, confidence interval; CP, corticomedullary phase; NP, nephrogenic phase; EP, excretory phase; model-1 =  $1 / [1 + e^{-(-3.831 \text{ gross hematuria} + 3.206 \text{ microscopic hematuria} + 2.783 \text{ infiltrative growth pattern} - 3.416 \text{ heterogeneous enhancement} - 0.698)}]$ .

**Table 2.** Univariate and multivariate logistic regression analyses of the CT and clinical features for ECCRCC or ERUC

Variables	Univariate logistic regression			Multivariate logistic regression		
	P	OR	95% CI	P	OR	95% CI
<b>Heterogeneous enhancement</b>						
Yes	<.001	0.089	0.026-0.300	.005	0.027	0.002-0.342
No		Ref. (1.000)			Ref. (1.000)	
<b>Hematuria</b>						
Gross	<.001	15.750	3.601-68.884	.003	53.995	3.987-731.168
Microscopic	.066	3.938	0.911-17.014	.027	31.126	1.490-650.085
No		Ref. (1.000)			Ref. (1.000)	
<b>Infiltrative growth pattern</b>						
Bean	.001	13.722	2.837-66.361	.022	24.301	1.586-372.402
Ball		Ref. (1.000)			Ref. (1.000)	
<b>Pseudo-capsule sign</b>						
Yes	.005	0.105	0.022-0.507	.631	1.980	0.122-32.204
No		Ref. (1.000)			Ref. (1.000)	
<b>Hydronephrosis</b>						
Yes	.004	5.185	1.670-16.009			
No		Ref. (1.000)				
<b>Necrosis</b>						
Extensive	.044	0.098	0.010-0.936			
Local	.016	0.071	0.008-0.605			
No		Ref. (1.000)				
<b>Renal calculus</b>						
Yes	.016	4.800	1.332-17.291			
No		Ref. (1.000)				
<b>Flank pain</b>						
Yes	.038	3.176	1.066-9.462			
No		Ref. (1.000)				
Age	.001	0.894	0.839-0.953			
CP	<.001	1.142	1.062-1.229			
NP	.001	1.095	1.039-1.155			
EP	.005	1.098	1.028-1.173			

When calculating OR values of variables with 3 categories (hematuria and necrosis), the categories of gross hematuria/extensive necrosis and microscopic hematuria/ local necrosis were compared against no hematuria/ no necrosis, respectively.

CT, computed tomography; ECCRCC, endophytic clear cell renal cell carcinoma; ERUC, endophytic renal urothelial carcinoma; OR, odds ratio; Ref, reference; CP, corticomedullary phase (tumor); NP, nephrogenic phase (tumor); EP, excretory phase (tumor).

(AUC = 0.938, sensitivity = 84.10%, specificity = 95.20%,  $P < .001$ ) were presented (Table 1) (Figure 4).

## Discussion

The reported incidence of CSI in RCC is 3%–14%.<sup>11,13,15,33,34</sup> To the best of our knowledge, the incidence of CSI has not been reported specifically in ccRCC. In our study, the incidence of CSI in ccRCC was approximately 46.54% (289/621) and that of ECCRCC among ccRCCs was approximately

15.22% (44/289). Endophytic renal neoplasms are different from those present in CSI. ECCRCC is one of the ccRCCs included with CSI, although most CSIs are exophytic tumors. Tumors that are centrally located in the renal pelvis are usually urothelial neoplasms, especially UC.<sup>8</sup> In this study, the incidence of RUC among all the cases of UC was approximately 14.08% (165/1.172), while the incidence of ERUC among all cases of RUC was approximately 12.73% (21/165). Previous reports of the CT features of RUC did not include

flowcharts depicting the selection of the patients.<sup>9,10,35</sup>

The description and characteristics of ERUC cases in the present study differed in certain ways from those in previous studies. In the present ERUC cases, renal calculi and hydronephrosis were recorded, which were not mentioned in 3 previous reports,<sup>9,10,35</sup> and were reported only as unusual imaging manifestations by Prado et al.<sup>36</sup>

Zhu et al.<sup>35</sup> reported a few RUCs with necrosis, whereas Raza et al.<sup>9</sup> did not mention the number of necrosis. Moreover, we

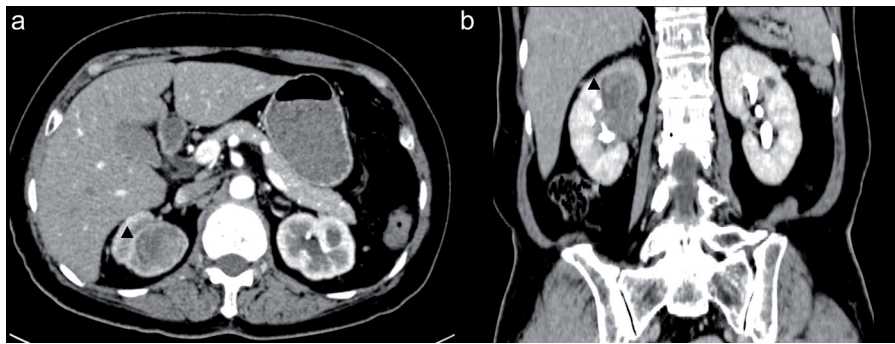


**Figure 7.** A 74-year-old woman with ERUC. Contrast-enhanced CT: axial image in the corticomedullary phase (a) and coronal image in the excretory phase (b) show an endophytic, mild heterogeneously enhanced mass in the right kidney. A part of the interface between the mass and the renal parenchyma is poorly defined, with a pseudo-capsule sign around the tumor (black arrowhead).

observed higher incidence of flank pain and hematuria in the present cases of ERUC as compared to that of previous reports. These differences may be attributable to the study populations, including the difference in lifestyle factors. Another reason may be the larger size of UC cases in our study compared to others.

In our study, heterogeneous enhancement, hematuria, and the infiltrative growth pattern were independent predictors of ECCRCC vs. ERUC. The predictive model was able to distinguish ECCRCC from ERUC; a diagnosis of ERUC was more likely with homogeneous enhancement, hematuria, and an infiltrative growth pattern (Table 2) (Figure 4). In this study, ECCRCC (Figures 2b, 5) was more susceptible to a distinct heterogeneous enhancement than ERUC (Figures 2a, 6), which was consistent with previous reports.<sup>9,10</sup> This may be caused by the rich blood supply and susceptibility to hemorrhage and necrosis in ECCRCCs. A larger ccRCC is reportedly prone to necrosis and heterogeneous enhancement.<sup>26,37,38</sup> Furthermore, our clinical data revealed that patients with ERUC were more susceptible to hematuria (both gross and microscopic) than those with ECCRCC. Intermittent microscopic hematuria may be missed upon clinical examination. Additionally, a bean shape and a ball shape corresponded to the patterns of mass infiltrative growth and expansive growth in the renal parenchyma, respectively.<sup>25</sup> ERUC tended to invade the renal parenchyma with an infiltrative growth pattern (Figure 6), whereas ECCRCC tended to expand in an expansive growth pattern in the renal parenchyma (Figure 5), similar to previous findings.<sup>9</sup>

Although age, CP, NP, EP, and the pseudo-capsule sign were excluded

from the predictive model, they may be of some assistance in the differentiation of ECCRCC from ERUC during a clinical examination. Similar to previous reports, patients with ECCRCC in this study were younger than those with ERUC.<sup>9,10</sup> Shariat et al.<sup>39</sup> reported a peak incidence of upper urinary tract UC in individuals aged 70-90 years. In the study by Bata et al.,<sup>10</sup> the attenuation of ccRCC was significantly higher than that of RUC in CP and NP. However, in our study, the attenuation of ECCRCC was significantly higher than that of ERUC for each phase of CT dynamic contrast-enhanced scanning. The hyperenhancement of ECCRCC and the hypoenhancement of ERUC in the CP may be attributed to the hypervascular nature of ECCRCC and the hypovascular nature of ERUC. In addition, 2 patients with ERUC in our study exhibited pseudo-capsule signs (Figure 7), which has not been reported before. However, the pseudo-capsule sign in patients with ERUC differed from that in patients with ECCRCC (Figure 5a and c). The former was the compression of renal pelvis fat, while the latter was the deposition of fibrous tissue after compression, leading to ischemic necrosis.<sup>40</sup>

Our study has certain limitations. First, we analyzed and compared the clinical and CT characteristics of patients with ERUC and ECCRCC only, without investigating other RCC subtypes. Second, although this study included a larger sample of patients with ECCRCC and ERUC than that in previous studies, the sample size remains small, which would inevitably lead to statistical bias. Further studies with larger samples are required to validate the results of our study. Third, our study considered the diagnosis only, not the prognosis.

In brief, our predictive model, which incorporates CT and clinical characteristics, may assist in the differential diagnosis of ECCRCC and ERUC. Endophytic renal tumors with an expansive growth pattern, distinct heterogeneous enhancement, and no hematuria may be considered ECCRCC. Moreover, cases in which patients are younger and exhibit hyperenhancement and the pseudo-capsule sign should be more supported for consideration as ECCRCC.

## Acknowledgments

The authors thank Professor Saojun Li from the School of Public Health of Guangxi Medical University for her comments and guidance in statistical analysis.

## Conflict of interest disclosure

The authors declared no conflicts of interest.

## References

- Capitanio U, Bensalah K, Bex A, et al. Epidemiology of renal cell carcinoma. *Eur Urol*. 2019; 75(1):74-84. [CrossRef]
- Gervais DA, McGovern FJ, Wood BJ, Goldberg SN, McDougal WS, Mueller PR. Radiofrequency ablation of renal cell carcinoma: early clinical experience. *Radiology*. 2000; 217(3):665-672. [CrossRef]
- Weiss LM, Gelb AB, Medeiros LJ. Adult renal epithelial neoplasms. *Am J Clin Pathol*. 1995; 103(5):624-635. [CrossRef]
- Shuch B, Hofmann JN, Merino MJ, et al. Pathologic validation of renal cell carcinoma histology in the surveillance, epidemiology, and end results program. *Urol Oncol*. 2014;32(1):23.e9-23.13. [CrossRef]
- Truong LD, Shen SS. Immunohistochemical diagnosis of renal neoplasms. *Arch Pathol Lab Med*. 2011;135(1):92-109. [CrossRef]
- Li Y, Ding YU, Chen D, et al. Renal cell carcinoma growing into the renal pelvis and mimicking transitional cell carcinoma: A case report and literature review. *Oncol Lett*. 2015; 9(4):1869-1872. [CrossRef]
- Jeong YB, Kim HJ. Is it transitional cell carcinoma or renal cell carcinoma on computed tomography image? *Urology*. 2012;79(3):e42-e43. [CrossRef]
- Rouprêt M, Babjuk M, Burger M, et al. European Association of Urology guidelines on upper urinary tract urothelial carcinoma: 2020 update. *Eur Urol*. 2021;79(1):62-79. [CrossRef]
- Raza SA, Sohaib SA, Sahdev A, et al. Centrally infiltrating renal masses on CT: differentiating intrarenal transitional cell carcinoma from centrally located renal cell carcinoma. *AJR Am J Roentgenol*. 2012;198(4):846-853. [CrossRef]
- Bata P, Tarnoki DL, Tarnoki AD, et al. Transitional cell and clear cell renal carcinoma: differentiation of distinct histological types with multiphase CT. *Acta Radiol*. 2014;55(9):1112-1119. [CrossRef]

11. Karlo CA, Di Paolo PL, Hricak H, Tickoo SK, Russo P, Akin O. CT of renal cell carcinoma: assessment of collecting system invasion. *AJR Am J Roentgenol.* 2013;201(6):W821-W827. [\[CrossRef\]](#)
12. Verhoest G, Avakian R, Bensalah K, et al. Urinary collecting system invasion is an independent prognostic factor of organ confined renal cell carcinoma. *J Urol.* 2009;182(3):854-859. [\[CrossRef\]](#)
13. Terrone C, Cracco C, Guercio S, et al. Prognostic value of the involvement of the urinary collecting system in renal cell carcinoma. *Eur Urol.* 2004;46(4):472-476. [\[CrossRef\]](#)
14. Klatte T, Chung J, Leppert JT, et al. Prognostic relevance of capsular involvement and collecting system invasion in stage I and II renal cell carcinoma. *BJU Int.* 2007;99(4):821-824. [\[CrossRef\]](#)
15. Takamatsu A, Yoshida K, Obokata M, et al. Urinary collecting system invasion on multiphasic CT in renal cell carcinomas: incidence, characteristics, and clinical significance. *Abdom Radiol (NY).* 2021;46(5):2090-2096. [\[CrossRef\]](#)
16. Van Dd Pol JAA, George L, Van Den Brandt PA, et al. Etiologic heterogeneity of clear-cell and papillary renal cell carcinoma in the Netherlands Cohort Study. *Int J Cancer.* 2021; 148:67-76.
17. Colin P, Koenig P, Ouzzane A, et al. Environmental factors involved in carcinogenesis of urothelial cell carcinomas of the upper urinary tract. *BJU Int.* 2009;104(10):1436-1440. [\[CrossRef\]](#)
18. Van de Pol JAA, Van den Brandt PA, Schouten LJ. Kidney stones and the risk of renal cell carcinoma and upper tract urothelial carcinoma: the Netherlands cohort study. *Br J Cancer.* 2019;120(3):368-374. [\[CrossRef\]](#)
19. Chou YH, Huang CN, Li WM, et al. Clinical study of ammonium acid urate urolithiasis. *Kaohsiung J Med Sci.* 2012;28(5):259-264. [\[CrossRef\]](#)
20. Lorenzo-Gómez MF, Padilla-Fernández B, Antúnez-Plaza P, Gracia-Criado FJ, Mirón-Canelo JA, Silva Abuín JM. Clinical profile and epidemiological changes of clear cell renal carcinoma during 12 years in our health area. *Arch Esp Urol.* 2012;65(9):823-829.
21. Cowan NC. CT urography for hematuria. *Nat Rev Urol.* 2012;9(4):218-226. [\[CrossRef\]](#)
22. Ito Y, Kikuchi E, Tanaka N, et al. Preoperative hydronephrosis grade independently predicts worse pathological outcomes in patients undergoing nephroureterectomy for upper tract urothelial carcinoma. *J Urol.* 2011;185(5): 1621-1626. [\[CrossRef\]](#)
23. Shinagare AB, Davenport MS, Park H, et al. Lexicon for renal mass terms at CT and MRI: A consensus of the society of abdominal radiology disease-focused panel on renal cell carcinoma. *Abdom Radiol (NY).* 2021;46(2):703-722. [\[CrossRef\]](#)
24. Shinagare AB, Vikram R, Jaffe C, et al. Radiogenomics of clear cell renal cell carcinoma: preliminary findings of the Cancer Genome Atlas-Renal Cell Carcinoma (TCGA-RCC) Imaging Research Group. *Abdom Imaging.* 2015;40(6): 1684-1692. [\[CrossRef\]](#)
25. Dyer R, DiSantis DJ, McClennan BL. Simplified imaging approach for evaluation of the solid renal mass in adults. *Radiology.* 2008;247(2):331-343. [\[CrossRef\]](#)
26. Paño B, Macías N, Salvador R, et al. Usefulness of MDCT to differentiate Between renal cell carcinoma and oncocytoma: development of a predictive model. *AJR Am J Roentgenol.* 2016;206(4):764-774. [\[CrossRef\]](#)
27. Jung SC, Kim SH, Cho JY. A comparison of the use of contrast media with different iodine concentrations for multidetector CT of the kidney. *Korean J Radiol.* 2011;12(6):714-721. [\[CrossRef\]](#)
28. Swets JA. Measuring the accuracy of diagnostic systems. *Science.* 1988;240(4857):1285-1293. [\[CrossRef\]](#)
29. Nick TG, Campbell KM. Logistic regression. In: Ambrosius W. T., ed. *Topics in Biostatistics.* New York: Humana; 2007:277-278.
30. Hill AB. The environment and disease: association or causation? *Proc R Soc Med.* 1965;58:295-300. [\[CrossRef\]](#)
31. Livesey G, Taylor R, Livesey HF, et al. Dietary glycemic index and load and the risk of Type 2 diabetes: assessment of causal relations. *Nutrients.* 2019;11(6):1436. [\[CrossRef\]](#)
32. CRAMER JS. The early origins of the logit model. *Stud Hist Philos Sci C.* 2004;35(4):613-626. [\[CrossRef\]](#)
33. Schrader AJ, Rustemeier J, Varga Z, et al. Urinary collecting system invasion in renal cell carcinoma: incidence and long-term prognosis. *Int J Urol.* 2009;16(9):718-722. [\[CrossRef\]](#)
34. Uzzo RG, Cherullo E, Myles J, Novick AC. Renal cell carcinoma invading the urinary collecting system: implications for staging. *J Urol.* 2002;167(6):2392-2396. [\[CrossRef\]](#)
35. Zhu Q, Zhu W, Wu J, Chen W. Multidetector CT imaging features of invasive renal parenchyma urothelial carcinoma. *Br J Radiol.* 2016;89(1063): 20151068. [\[CrossRef\]](#)
36. Prando A, Prando P, Prando D. Urothelial cancer of the renal pelvicaliceal system: unusual imaging manifestations. *RadioGraphics.* 2010; 30(6):1553-1566. [\[CrossRef\]](#)
37. Lam JS, Shvarts O, Said JW, et al. Clinicopathologic and molecular correlations of necrosis in the primary tumor of patients with renal cell carcinoma. *Cancer.* 2005;103(12):2517-2525. [\[CrossRef\]](#)
38. Jiang J, Chen Y, Zhou Y, Zhang H. Clear cell renal cell carcinoma: contrast-enhanced ultrasound features relation to tumor size. *Eur J Radiol.* 2010;73(1):162-167. [\[CrossRef\]](#)
39. Shariat SF, Favaretto RL, Gupta A, et al. Gender differences in radical nephroureterectomy for upper tract urothelial carcinoma. *World J Urol.* 2011;29(4):481-486. [\[CrossRef\]](#)
40. Tsili AC, Argyropoulou MI, Gousia A, et al. Renal cell carcinoma: value of multiphase MDCT with multiplanar reformations in the detection of pseudocapsule. *AJR Am J Roentgenol.* 2012; 199(2):379-386. [\[CrossRef\]](#)



**Supplementary Table 1.** Inter-rater agreement of the 2 readers as measured by intraclass correlation coefficient

Characteristics	ICC	95% CI	<i>P</i>
Size	0.935	0.910-0.966	.009
UP	0.834	0.776-0.878	<.001
CP	0.851	0.801-0.892	<.001
NP	0.881	0.593-0.969	<.001
EP	0.927	0.883-0.955	<.001

ICC, intraclass correlation coefficient; UP, unenhanced phase; CP, corticomedullary phase; NP, nephrographic phase; EP, excretory phase.

**Supplementary Table 2.** Inter-rater agreement of the 2 readers as measured by kappa statistics

Characteristics	Kappa	95% CI	<i>P</i>
Infiltrative growth pattern	0.844	0.713-0.975	<.001
Pseudo-capsule sign	0.863	0.734-0.992	<.001
Preserving reniform contour	0.815	0.674-0.956	<.001
Perinephric stranding	0.851	0.710-0.992	<.001
Hydronephrosis	0.930	0.834-1.000	<.001
Necrosis	0.928	0.848-1.000	<.001
Heterogeneous enhancement	0.833	0.694-0.972	<.001
Calcification	0.920	0.812-1.000	<.001
Renal calculus	0.909	0.786-1.000	<.001
Renal vein invasion	0.860	0.707-1.000	<.001
Lymphatic metastasis	0.858	0.666-1.000	<.001
Distant metastasis	0.840	0.622-1.000	<.001

**Supplementary Table 3.** Clinical characteristics of patients with ECCRCC and ERUC

Characteristics	ECCRCC (n = 44)	ERUC (n = 21)	<i>P</i>
	Median (range)/n (%)	Median (range)/n (%)	
Sex			
Male	35 (79.55)	17 (80.95)	1.000
Female	9 (20.45)	4 (19.05)	
Age (years)	55 (48.25-59.50)	68 (63.00-73.00)	<.001
Smoking history	12 (27.27)	6 (28.57)	.913
Flank pain	17 (38.64)	14 (66.67)	.034
History of kidney stones	8 (18.18)	7 (33.33)	.214
Hematuria			
Gross hematuria	8 (18.18)	14 (66.67)	<.001
Microscopic hematuria	9 (20.45)	4 (19.05)	

ECCRCC, endophytic clear cell renal cell carcinoma; ERUC, endophytic renal urothelial carcinoma.

**Supplementary Table 4.** CT characteristics of patients with ECCRCC and ERUC

Characteristics	ECCRCC (n=44)	ERUC (n=21)	P
	Median (range)/mean ± SD/n (%)	Median (range)/ mean ± SD/n (%)	
Side, n (%)			
Left	28 (63.64)	11 (52.38)	.386
Right	16 (36.36)	10 (47.62)	
Size (cm)	43.20 (32.70-68.70)	44.37 (33.32-59.20)	.768
Preserving reniform contour	21 (47.73)	10 (47.62)	.993
Perinephric stranding	10 (22.73)	9 (42.86)	.095
Infiltrative growth pattern			
Bean shape	18 (40.91)	19 (90.48)	<.001
Ball shape	26 (59.09)	2 (9.52)	
Pseudo-capsule sign	22 (50.00)	2 (9.52)	.002
Hydronephrosis	9 (20.45)	12 (57.14)	.003
Necrosis			
Extensive (≥50%)	17 (38.64)	1 (4.76)	.009
Local (<50%)	17 (38.64)	14 (66.67)	
Heterogeneous enhancement	36 (81.82)	6 (28.57)	<.001
Calcification	14 (31.82)	3 (14.29)	.133
Renal calculus	5 (11.36)	8 (38.10)	.019
Renal vein invasion	6 (13.64)	6 (28.57)	.180
Lymphatic node metastasis	3 (6.82)	4 (19.05)	.200
Distant metastasis	3 (6.82)	4 (19.05)	.200
UP (HU)	36.67 ± 6.02	36.25 ± 3.68	.063
CP (HU)	103.07 (82.6-126.08)	62.59 (54.64-66.7)	<.001
NP (HU)	94.76 (79-110.76)	77.94 (65.76-79.68)	<.001
EP (HU)	73.70 (66.74-87.54)	64.75 (58.43-73.49)	.002

CT, computed tomography; ECCRCC, endophytic clear cell renal carcinoma; ERUC, endophytic renal urothelial carcinoma; SD, standard deviation; UP, unenhanced phase; HU, Hounsfield units; CP, corticomedullary phase; NP, nephrogenic phase; EP, excretory phase.

**Supplementary Table 5.** Variable assignments before logistic regression analysis

Assignment	Tumor	HE	Hematuria	IGP	PcS	Hydronephrosis	Necrosis	RC	FP
2			GH				EN		
1	ECCRCC	Yes	MH	Bean shape	Yes	Yes	LN	Yes	Yes
0	ERUC	No	No	Ball shape	No	No	No	No	No

HE, heterogeneous enhancement; IGP, infiltrative growth pattern; PcS, pseudo-capsule sign; RC, renal calculus; FP, flank pain; ECCRCC, endophytic clear cell renal cell carcinoma; GH, gross hematuria; EN, extensive necrosis; MH, microscopic hematuria; LN, local necrosis; ERUC, endophytic renal urothelial carcinoma.

**Supplementary Table 6.** Multivariable logistic regression analyses (construction of the prediction model) of CT findings and clinical data for differentiation of ECCRCC and ERUC

	$\beta$	P	OR	95% CI
Heterogeneous enhancement	-3.416	.004	0.033	0.003-0.330
Infiltrative growth pattern	2.783	.008	16.171	2.083-125.527
Gross hematuria	3.831	.002	46.120	3.959-537.244
Microscopic hematuria	3.206	.023	24.671	1.553-391.852
Constant	-0.698	.334	0.498	

CT, computed tomography; ECCRCC, endophytic clear cell renal cell carcinoma; ERUC, endophytic renal urothelial carcinoma.

**Supplementary Equation 1. Equation of the prediction model.**

$$\text{Logit}(p) = \text{Ln} [p/(1-p)]$$

$p$ , the probabilistic predictive value